

Supplementary Materials for “Theoretical Prediction on the Structures and Stability of the Noble-Gas Containing Anions FN<sub>g</sub>CC<sup>-</sup> (Ng = He, Ar, Kr, and Xe)”

**Chia-Yu Peng, Chang-Yu Yang, Yi-Lun Sun, Wei-Ping Hu\***

*Department of Chemistry and Biochemistry, National Chung Cheng University  
Chia-Yi, Taiwan 621*

E-mail: [chewph@ccu.edu.tw](mailto:chewph@ccu.edu.tw)

6 Tables, 8 Figures.

Submitted to *J. Chem. Phys.*, October, 2012.

### CASSCF and CASPT2 calculations:

For FHeCC<sup>-</sup>, the active space consists of 16 electrons in 12 orbitals (16,12), where all the valence electrons and orbitals except the 2s electrons and 2s orbital of the fluorine atom are included in the active space. For FN<sub>g</sub>CC<sup>-</sup>, Ng = Ar, Kr, and Xe, the active space consists of 20 electrons in 14 orbitals (20,14) where all the valence electrons and orbitals except the 2s electrons and orbital of the fluorine atom, and the *ns* (*n* = 3, 4, 5) electrons and orbital of the noble gas atom are included in the active space.

TABLE S1. Calculated bond lengths (Å) and bond angles(°) of TS3 for FHeCC<sup>-</sup>.

Method	F–He	He–C1	C1–C2	F–He–C1	He–C1–C2
MP2/apdz	1.693	1.474	1.315	180.0	180.0
MP2/aptz	1.682	1.523	1.297	180.0	180.0
CCSD(T)/aptz	1.723	1.461	1.281	179.0	147.4

TABLE S2. Calculated energy difference between triplet and singlet CC (kcal/mol).

Method	E[CC(T) – CC(S)]
B3LYP/aptz	-23.0
MPW1PW91/aptz	-25.5
MP2/apdz	4.2
MP2/aptz	6.6
CCSD(T)/aptz	1.6
Expt. <sup>a</sup>	2.0 ± 1.0

<sup>a</sup>The experimental S-T gap was taken from Ref 65.

TABLE S3. Calculated energies of NgCC relative to Ng + CC (kcal/mol).

Ng =	He	Ar	Kr	Xe
B3LYP/aptz	0.0	-1.6	-8.2	-20.9
MPW1PW91/aptz	0.0	-2.3	-11.7	-25.3
MP2/apdz	-0.1	-1.2	-2.2	-4.2
MP2/aptz	-0.1	-1.2	-2.4	-4.9
CCSD(T)/aptz//B3LYP/aptz	0.0	2.9	11.3	-1.0
CCSD(T)/aptz//MP2/apdz	-0.1	-0.4	-1.1	-2.9
CCSD(T)/aptz//MP2/aptz	-0.1	-0.4	-1.0	-3.1
CCSD(T)/aptz		-0.5	-1.1	-5.0
CASPT2/aptz		4.5	-5.2	-1.2

TABLE S4. Calculated bond lengths ( $\text{\AA}$ ) and bond angles( $^\circ$ ) of NgCC.

Method	Ng–C	C–C	Ng–C–C
HeCC			
B3LYP/aptz	6.108	1.247	180.0
MPW1PW91/aptz	3.752	1.246	180.0
MP2/apdz	3.186	1.278	180.0
MP2/aptz	3.222	1.260	180.0
ArCC			
B3LYP/aptz	2.446	1.250	180.0
MPW1PW91/aptz	2.149	1.250	180.0
MP2/apdz	3.101	1.279	180.0
MP2/aptz	3.061	1.261	180.0
CCSD(T)/aptz	3.662	1.251	163.8
CASPT2/aptz	2.270	1.305	180.0
KrCC			
B3LYP/aptz	2.151	1.263	143.8
MPW1PW91/aptz	1.955	1.258	149.4
MP2/apdz	3.049	1.280	180.0
MP2/aptz	2.992	1.262	180.0
CCSD(T)/aptz	3.151	1.252	173.7
CASPT2/aptz	2.653	1.256	180.0
XeCC			
B3LYP/aptz	2.106	1.257	151.3
MPW1PW91/aptz	2.057	1.252	159.4
MP2/apdz	3.005	1.284	180.0
MP2/aptz	2.976	1.267	180.0
CCSD(T)/aptz	2.528	1.256	180.0
CASPT2/aptz	2.481	1.263	180.0

TABLE S5. Calculated relative energies<sup>a</sup> (kcal/mol) of FN<sub>g</sub>O<sup>-</sup>.

	S-T gap <sup>b</sup>	Relative to F <sup>-</sup> + Ng + O(S)	Relative to F <sup>-</sup> + NgO	Relative to F + Ng + O <sup>-</sup>	Relative to F <sup>-</sup> + Ng + O(T)	Relative to FO <sup>-</sup> + Ng	Barrier <sup>c</sup>
<i>Ng = He</i>							
MP2/aug-cc-pVTZ	117.8	-39.4	NA <sup>d</sup>	-24.7	26.6	48.7	29.0 [25.0] <sup>e</sup>
MP2/aug-cc-pVQZ	121.4	-32.9	NA	-19.1	32.2	55.8	29.9 [26.0]
CCSD(T)/aug-cc-pVTZ	90.9	-23.6	NA	-18.4	27.3	50.9	22.1 [18.7]
CCSD(T)/aug-cc-pVQZ	91.1	-20.5	NA	-15.9	29.8	54.7	18.9
CCSD(T)/CBS <sup>f</sup>	94.4	-21.4	NA	-17.1	28.5	54.4	19.7
<i>Ng = Arg</i>							
MP2/aug-cc-pVTZ	65.1	-53.3	-31.9	-38.5	12.8	34.9	46.4 [44.8]
MP2/aug-cc-pVQZ	68.0	-54.9	-32.1	-41.0	10.2	33.9	47.9 [46.3]
CCSD(T)/aug-cc-pVTZ	41.6	-38.4	-30.3	-33.3	12.4	36.0	32.3 <sup>h</sup>
CCSD(T)/aug-cc-pVQZ	44.2	-39.4	-30.3	-34.8	10.9	35.8	33.3 <sup>h</sup>
CCSD(T)/CBS	46.1	-40.1	-30.4	-35.8	9.8	35.7	34.1 <sup>h</sup>
<i>Ng = Kr</i>							
MP2/aug-cc-pVTZ	72.2	-76.0	-39.5	-61.2	-9.9	12.2	65.5 [64.0]
MP2/aug-cc-pVQZ	74.3	-77.8	-39.9	-64.0	-12.7	10.9	66.9 [65.4]
CCSD(T)/aug-cc-pVTZ	52.7	-58.1	-37.4	-52.9	-7.3	16.4	49.0 <sup>h</sup>
CCSD(T)/aug-cc-pVQZ	54.5	-59.3	-37.7	-54.7	-9.0	15.9	49.9 <sup>h</sup>
CCSD(T)/CBS	55.9	-60.2	-38.0	-56.0	-10.3	15.5	50.6 <sup>h</sup>

	<i>Ng = Xe</i>						
MP2/aug-cc-pVTZ	77.2	-106.8	-48.6	-92.0	-40.7	-18.6	89.4 [88.1]
MP2/aug-cc-pVQZ	78.9	-109.8	-49.1	-96.0	-44.7	-21.1	91.0 [89.6]
CCSD(T)/aug-cc-pVTZ	63.3	-85.3	-45.9	-80.2	-34.5	-10.8	69.1 <sup>h</sup>
CCSD(T)/aug-cc-pVQZ	65.9	-87.9	-46.8	-83.2	-37.6	-12.6	70.8 <sup>h</sup>
CCSD(T)/CBS	67.8	-89.7	-47.5	-85.4	-39.8	-13.9	72.0 <sup>h</sup>

<sup>a</sup>Born-Oppenheimer energies, not including zero-point vibrational energies.

<sup>b</sup>Energy differences between the singlet and the triplet state at the optimized singlet-state geometry.

<sup>c</sup>Energy barriers for the FN<sub>g</sub>O<sup>-</sup> → FO<sup>-</sup> + Ng reactions.

<sup>d</sup>Not applicable. The HeO molecule is not an energy minimum.

<sup>e</sup>Values in parentheses including vibrational zero-point energies.

<sup>f</sup>Extrapolated results to the complete basis set limit using the aug-cc-pVTZ and aug-cc-pVQZ results and the inverse cubic formula by Halkier et al. [A. Halkier, T. Helgaker, P. Jørgensen, W. Klopper, H. Koch, J. Olsen, and A. K. Wilson, Chem. Phys. Lett. 286, 243 (1998).]

<sup>g</sup>The aug-cc-pV(*n+d*)Z basis sets were used for Ar.

<sup>h</sup>Single-point energy at MP2/aug-cc-pV(*T+d*)Z structure.

TABLE S6. Calculated bond lengths ( $\text{\AA}$ ) and bond angles( $^{\circ}$ ) of  $\text{FNgO}^-$ .

Method	FHeO <sup>-</sup>		FArO <sup>-</sup> <sup>b</sup>		FKrO <sup>-</sup>		FXeO <sup>-</sup>	
	F-He	He-O	F-Ar	Ar-O	F-Kr	Kr-O	F-Xe	Xe-O
MP2/apdz	1.637	1.055	2.242	1.710	2.251	1.817	2.290	1.957
MP2/aptz	1.606	1.043	2.194	1.673	2.211	1.786	2.269	1.919
MP2/apqz	1.601	1.038	2.180	1.666	2.198	1.780	2.258	1.910
CCSD(T)/aptz	1.626	1.110	2.226	1.765	2.259	1.854	2.305	1.953
CCSD(T)/apqz	1.621	1.100	2.224	1.754	2.261	1.842	2.286	1.938

<sup>a</sup> Linear structures for the all  $\text{FNgO}^-$  molecules.

<sup>b</sup>The aug-cc-pV(*n+d*)Z basis sets were used for Ar.

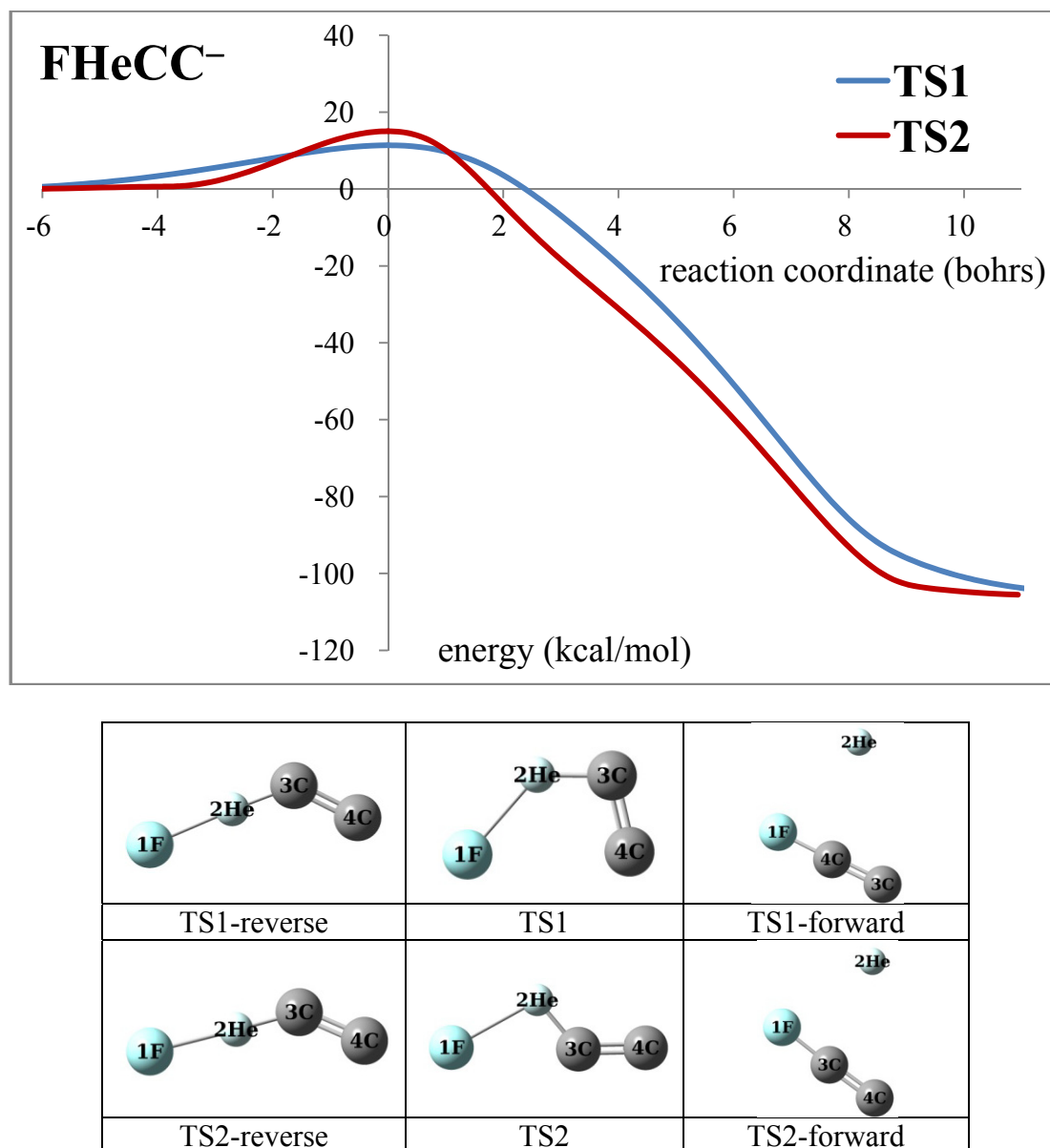


FIG. S1. Calculated potential energy curves along the reaction paths and structures of the TS and the end points in IRC calculation for FHeCC<sup>-</sup> at MPW1PW91/aug-cc-pVTZ level.

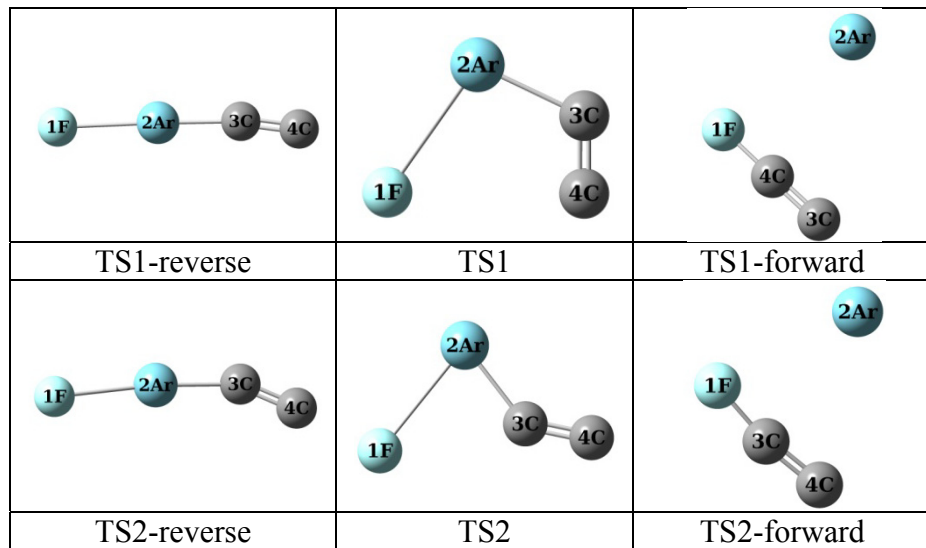
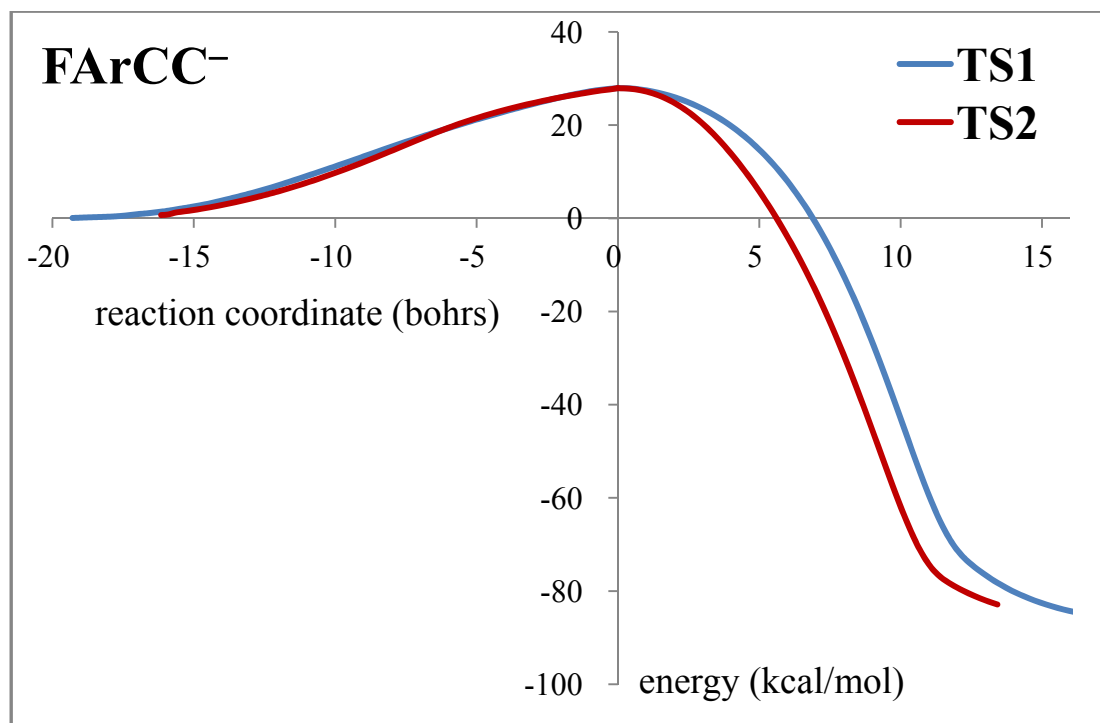


FIG. S2. Calculated potential energy curves along the reaction paths and structures of the TS and the end points in IRC calculation for FArCC<sup>-</sup> at MPW1PW91/aug-cc-pVTZ level.

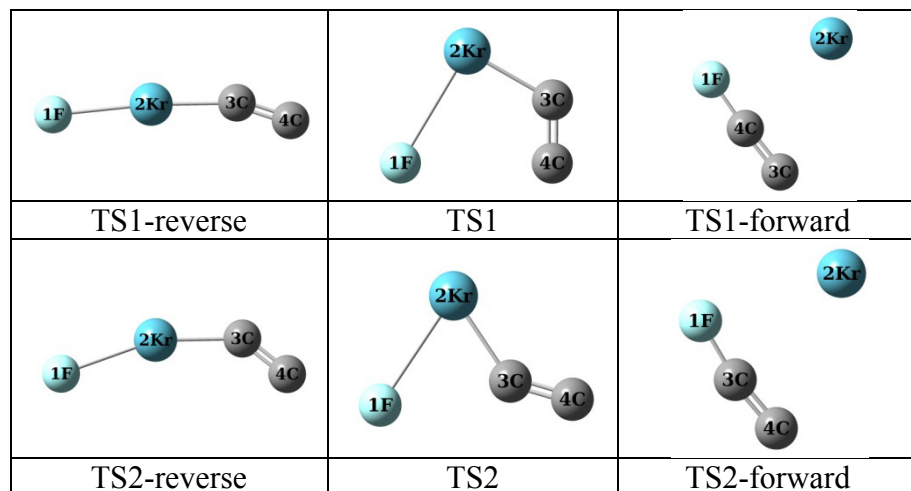
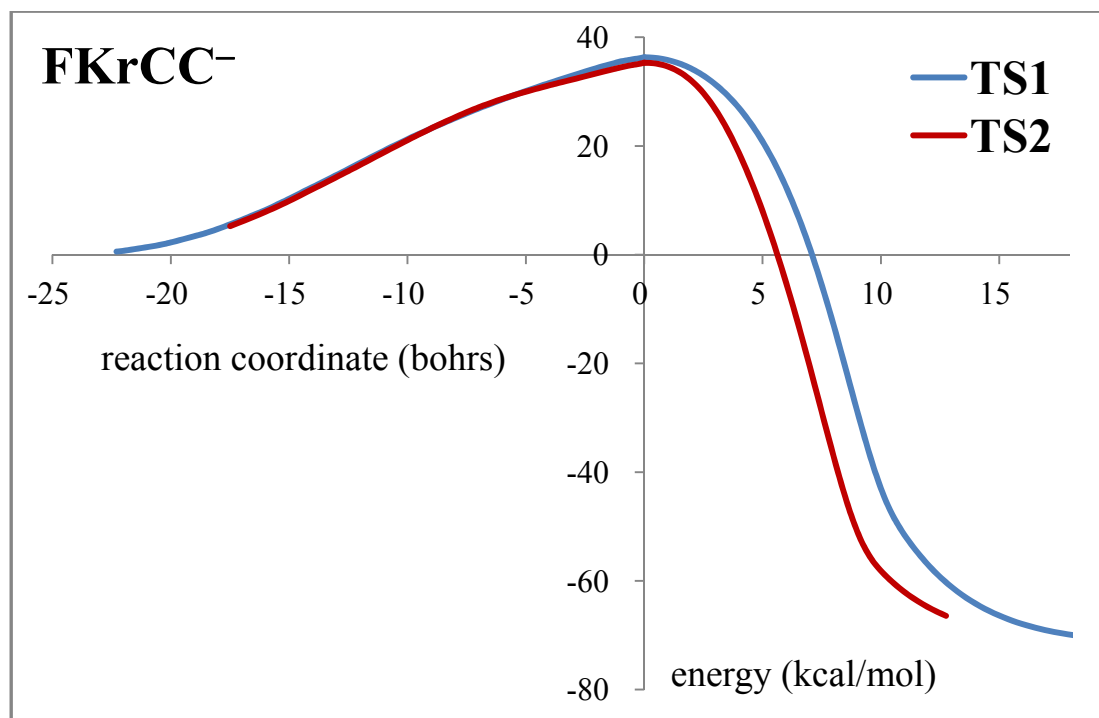


FIG. S3. Calculated potential energy curves along the reaction paths and structures of the TS and the end points in IRC calculation for FKrCC<sup>-</sup> at MPW1PW91/aug-cc-pVTZ level.

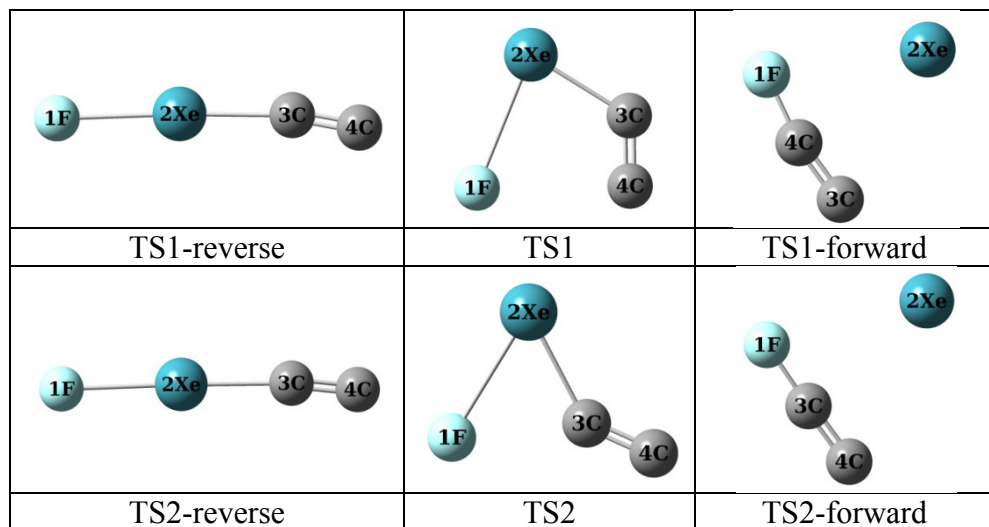
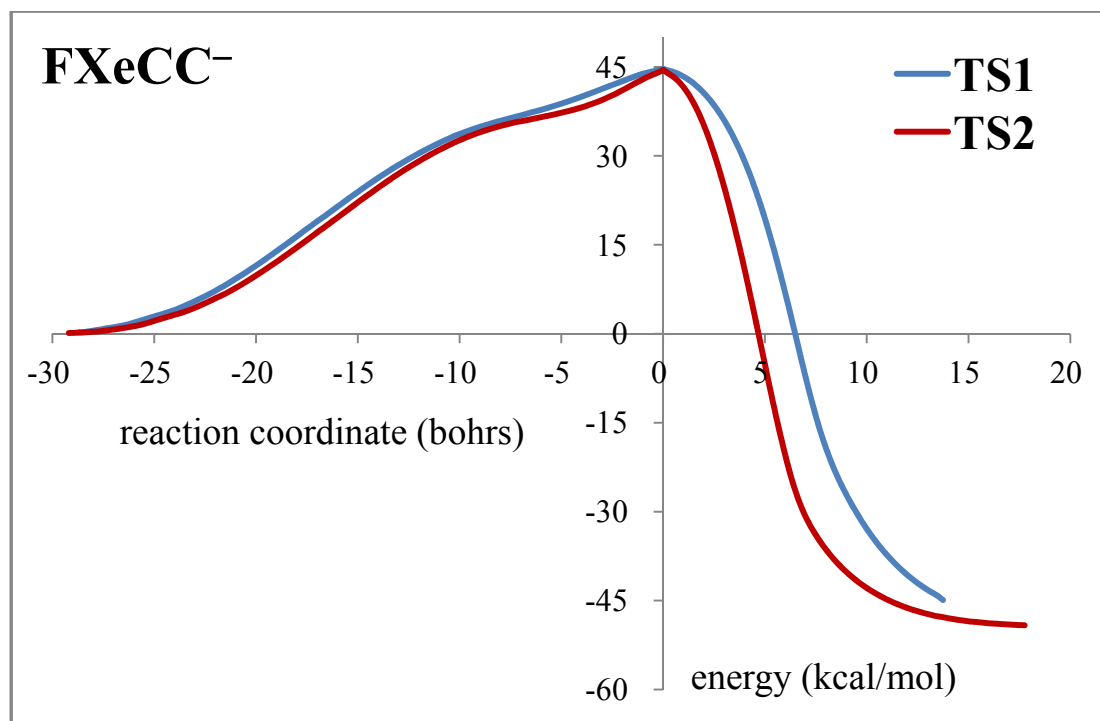


FIG. S4. Calculated potential energy curves along the reaction paths and structures of the TS and the end points in IRC calculation for FXeCC<sup>-</sup> at MPW1PW91/aug-cc-pVTZ level.

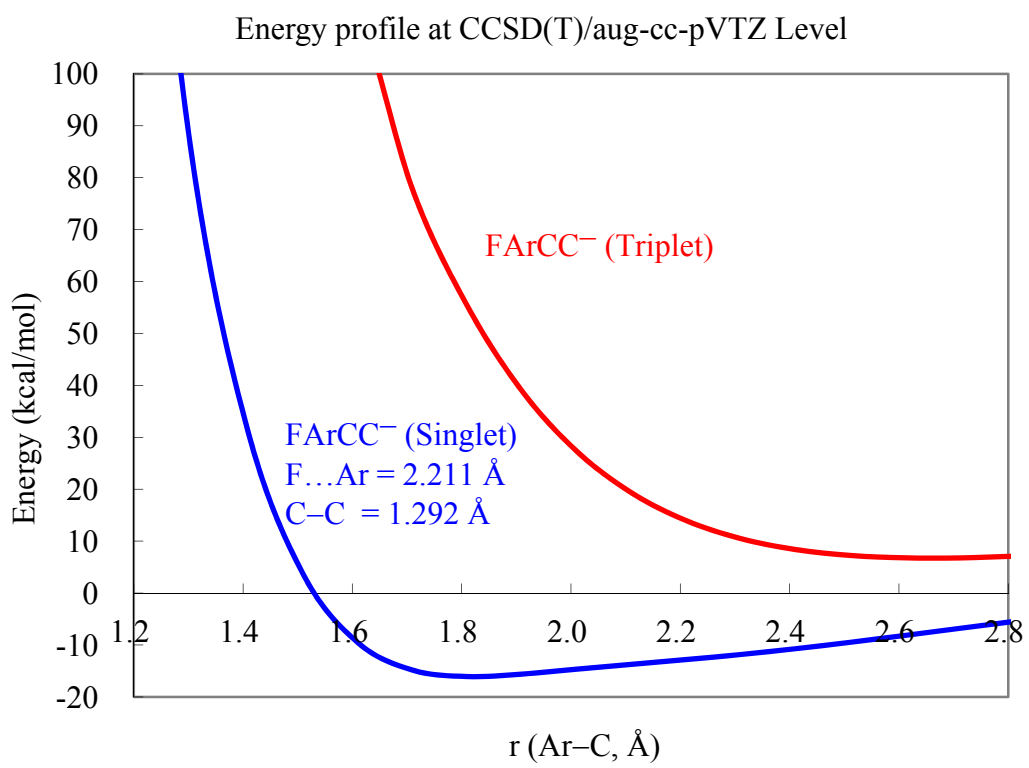


FIG. S5. The singlet and triplet energy curves along the Ar–C bond for FArCC<sup>−</sup>.

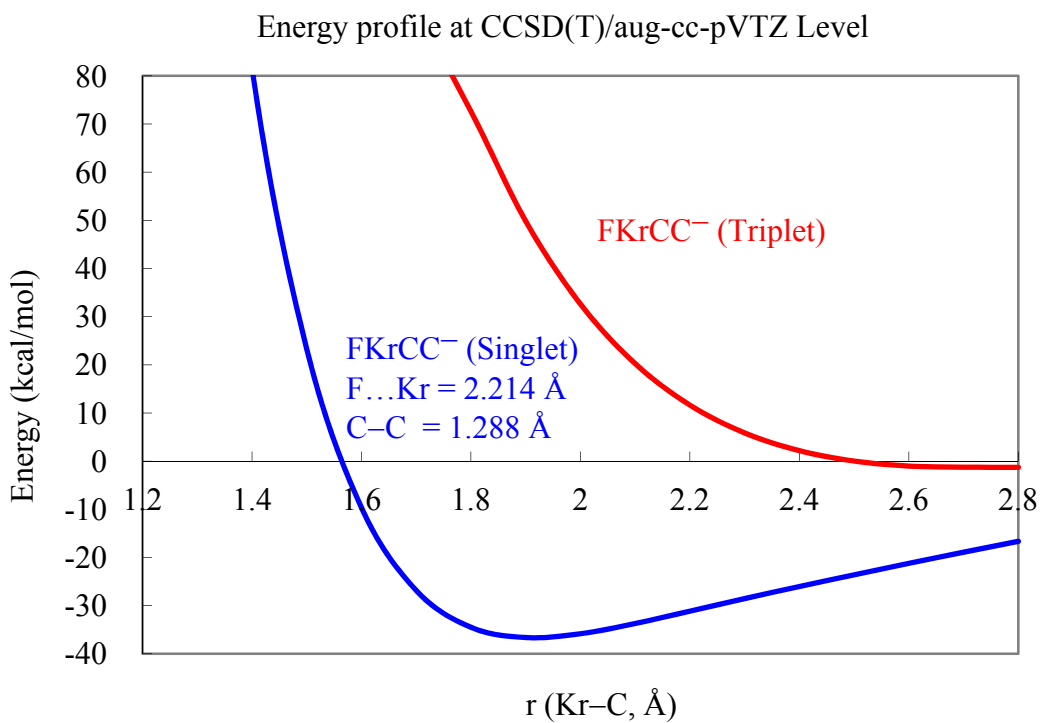


FIG. S6. The singlet and triplet energy curves along the Kr–C bond for  $\text{FKrCC}^-$ .

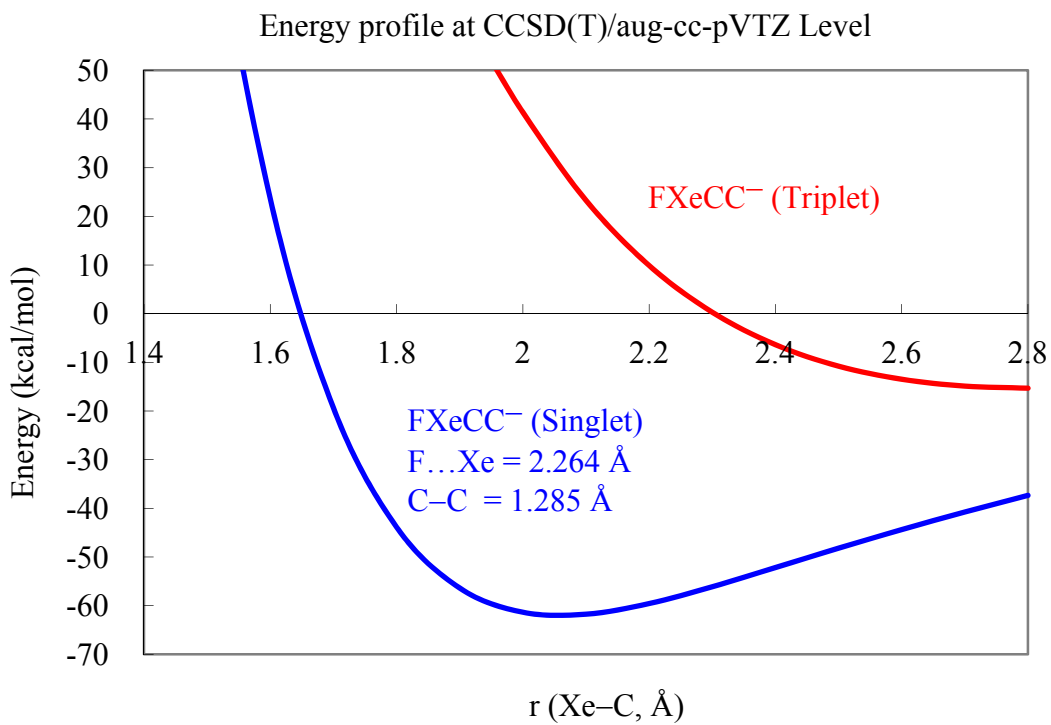


FIG. S7. The singlet and triplet energy curves along the Xe–C bond for FXeCC<sup>−</sup>.

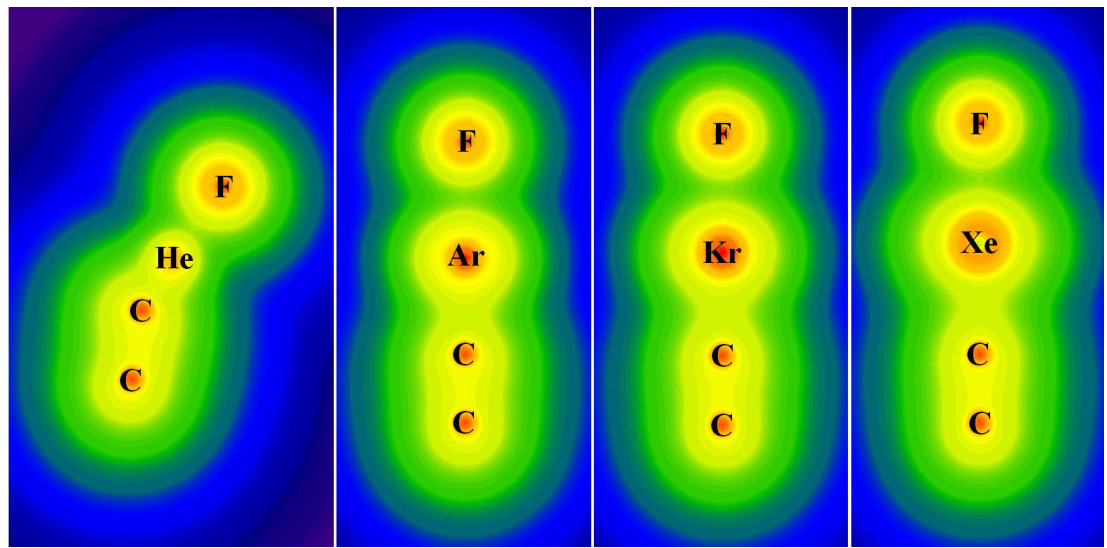


FIG. S8. Contour plots of the calculated electron density (MPW1PW91/aug-cc-pVTZ) of FHeCC<sup>-</sup>, FArCC<sup>-</sup>, FKrCC<sup>-</sup> and FXeCC<sup>-</sup>.